EUROPEAN LABORATORY FOR PARTICLE PHYSICS

CERN-PPE/97-05
10th January 1997

Study of $\phi(1020)$, $D^{*\pm}$ and B^* spin alignment in hadronic Z^0 decays

The OPAL Collaboration

Abstract

Measurements of helicity density matrix elements have been made for the $\phi(1020)$, $D^{*\pm}$ and B^* vector mesons in multihadronic Z^0 decays in the OPAL experiment at LEP. Results for inclusive ϕ produced with high energy show evidence for production preferentially in the helicity zero state, with $\rho_{00} = 0.54 \pm 0.08$, compared to the value of 1/3 expected for no spin alignment. The corresponding element for the $D^{*\pm}$ has a value of 0.40 ± 0.02, also suggesting a deviation from 1/3. The B^* result, with $\rho_{00} = 0.36 \pm 0.09$, is consistent with no spin alignment. Off-diagonal elements have been measured for the ϕ and D^* mesons; for the D^* the element $\mathrm{Re}\,\rho_{1-1}$ is non-zero, indicating non-independent fragmentation of the primary quarks.

Submitted to Zeitschrift für Physik C

The OPAL Collaboration

K. Ackerstaff[8], G. Alexander[23], J. Allison[16], N. Altekamp[5], K. Ametewee[25], K.J. Anderson[9], S. Anderson[12], S. Arcelli[2], S. Asai[24], D. Axen[29], G. Azuelos[18,a], A.H. Ball[17], E. Barberio[8], R.J. Barlow[16], R. Bartoldus[3], J.R. Batley[5], J. Bechtluft[14], C. Beeston[16], T. Behnke[8], A.N. Bell[1], K.W. Bell[20], G. Bella[23], S. Bentvelsen[8], P. Berlich[10], S. Bethke[14], O. Biebel[14], A. Biguzzi[5], S.D. Bird[16], V. Blobel[27], I.J. Bloodworth[1], J.E. Bloomer[1], M. Bobinski[10], P. Bock[11], H.M. Bosch[11], M. Boutemeur[34], B.T. Bouwens[12], S. Braibant[12], R.M. Brown[20], H.J. Burckhart[8], C. Burgard[8], R. Bürgin[10], P. Capiluppi[2], R.K. Carnegie[6], A.A. Carter[13], J.R. Carter[5], C.Y. Chang[17], D.G. Charlton[1,b], D. Chrisman[4], P.E.L. Clarke[15], S.G. Clowes[16], I. Cohen[23], J.E. Conboy[15], O.C. Cooke[16], M. Cuffiani[2], S. Dado[22], C. Dallapiccola[17], G.M. Dallavalle[2], S. De Jong[12], L.A. del Pozo[4], K. Desch[3], M.S. Dixit[7], E. do Couto e Silva[12], M. Doucet[18], E. Duchovni[26], G. Duckeck[34], I.P. Duerdoth[16], D. Eatough[16], J.E.G. Edwards[16], P.G. Estabrooks[6], H.G. Evans[9], M. Evans[13], F. Fabbri[2], M. Fanti[2], P. Fath[11], A.A. Faust[30], F. Fiedler[27], M. Fierro[2], H.M. Fischer[3], R. Folman[26], D.G. Fong[17], M. Foucher[17], A. Fürtjes[8], P. Gagnon[7], A. Gaidot[21], J.W. Gary[4], J. Gascon[18], S.M. Gascon-Shotkin[17], N.I. Geddes[20], C. Geich-Gimbel[3], F.X. Gentit[21], T. Geralis[20], G. Giacomelli[2], P. Giacomelli[4], R. Giacomelli[2], V. Gibson[5], W.R. Gibson[13], D.M. Gingrich[30,a], D. Glenzinski[9], J. Goldberg[22], M.J. Goodrick[5], W. Gorn[4], C. Grandi[2], E. Gross[26], J. Grunhaus[23], M. Gruwé[8], C. Hajdu[32], G.G. Hanson[12], M. Hansroul[8], M. Hapke[13], C.K. Hargrove[7], P.A. Hart[9], C. Hartmann[3], M. Hauschild[8], C.M. Hawkes[5], R. Hawkings[27], R.J. Hemingway[6], M. Herndon[17], G. Herten[10], R.D. Heuer[8], M.D. Hildreth[8], J.C. Hill[5], S.J. Hillier[1], T. Hilse[10], P.R. Hobson[25], R.J. Homer[1], A.K. Honma[28,a], D. Horváth[32,c], R. Howard[29], R.E. Hughes-Jones[16], D.E. Hutchcroft[5], P. Igo-Kemenes[11], D.C. Imrie[25], M.R. Ingram[16], K. Ishii[24], A. Jawahery[17], P.W. Jeffreys[20], H. Jeremie[18], M. Jimack[1], A. Joly[18], C.R. Jones[5], G. Jones[16], M. Jones[6], R.W.L. Jones[8], U. Jost[11], P. Jovanovic[1], T.R. Junk[8], D. Karlen[6], K. Kawagoe[24], T. Kawamoto[24], R.K. Keeler[28], R.G. Kellogg[17], B.W. Kennedy[20], J. Kirk[29], S. Kluth[8], T. Kobayashi[24], M. Kobel[10], D.S. Koetke[6], T.P. Kokott[3], M. Kolrep[10], S. Komamiya[24], T. Kress[11], P. Krieger[6], J. von Krogh[11], P. Kyberd[13], G.D. Lafferty[16], H. Lafoux[21], R. Lahmann[17], W.P. Lai[19], D. Lanske[14], J. Lauber[15], S.R. Lautenschlager[31], J.G. Layter[4], D. Lazic[22], A.M. Lee[31], E. Lefebvre[18], D. Lellouch[26], J. Letts[12], L. Levinson[26], C. Lewis[15], S.L. Lloyd[13], F.K. Loebinger[16], G.D. Long[28], M.J. Losty[7], J. Ludwig[10], A. Macchiolo[2], A. Macpherson[30], A. Malik[21], M. Mannelli[8], S. Marcellini[2], C. Markus[3], A.J. Martin[13], J.P. Martin[18], G. Martinez[17], T. Mashimo[24], W. Matthews[25], P. Mättig[3], W.J. McDonald[30], J. McKenna[29], E.A. Mckigney[15], T.J. McMahon[1], A.I. McNab[13], R.A. McPherson[8], F. Meijers[8], S. Menke[3], F.S. Merritt[9], H. Mes[7], J. Meyer[27], A. Michelini[2], G. Mikenberg[26], D.J. Miller[15], R. Mir[26], W. Mohr[10], A. Montanari[2], T. Mori[24], M. Morii[24], U. Müller[3], K. Nagai[26], I. Nakamura[24], H.A. Neal[8], B. Nellen[3], B. Nijjhar[16], R. Nisius[8], S.W. O'Neale[1], F.G. Oakham[7], F. Odorici[2], H.O. Ogren[12], N.J. Oldershaw[16], T. Omori[24], M.J. Oreglia[9], S. Orito[24], J. Pálinkás[33,d], G. Pásztor[32], J.R. Pater[16], G.N. Patrick[20], J. Patt[10], M.J. Pearce[1], S. Petzold[27], P. Pfeifenschneider[14], J.E. Pilcher[9], J. Pinfold[30], D.E. Plane[8], P. Poffenberger[28], B. Poli[2], A. Posthaus[3], H. Przysiezniak[30], D.L. Rees[1], D. Rigby[1], S. Robertson[28], S.A. Robins[13], N. Rodning[30], J.M. Roney[28], A. Rooke[15], E. Ros[8], A.M. Rossi[2], M. Rosvick[28], P. Routenburg[30], Y. Rozen[22], K. Runge[10], O. Runolfsson[8], U. Ruppel[14], D.R. Rust[12], R. Rylko[25], K. Sachs[10], E.K.G. Sarkisyan[23], M. Sasaki[24], C. Sbarra[29], A.D. Schaile[34], O. Schaile[34], F. Scharf[3], P. Scharff-Hansen[8], P. Schenk[34], B. Schmitt[8], S. Schmitt[11], M. Schröder[8],

H.C. Schultz-Coulon[10], M. Schulz[8], M. Schumacher[3], P. Schütz[3], W.G. Scott[20], T.G. Shears[16], B.C. Shen[4], C.H. Shepherd-Themistocleous[8], P. Sherwood[15], G.P. Siroli[2], A. Sittler[27], A. Skillman[15], A. Skuja[17], A.M. Smith[8], T.J. Smith[28], G.A. Snow[17], R. Sobie[28], S. Söldner-Rembold[10], R.W. Springer[30], M. Sproston[20], A. Stahl[3], M. Steiert[11], K. Stephens[16], J. Steuerer[27], B. Stockhausen[3], D. Strom[19], P. Szymanski[20], R. Tafirout[18], S.D. Talbot[1], S. Tanaka[24], P. Taras[18], S. Tarem[22], M. Thiergen[10], M.A. Thomson[8], E. von Törne[3], S. Towers[6], I. Trigger[18], T. Tsukamoto[24], E. Tsur[23], A.S. Turcot[9], M.F. Turner-Watson[8], P. Utzat[11], R. Van Kooten[12], G. Vasseur[21], M. Verzocchi[10], P. Vikas[18], M. Vincter[28], E.H. Vokurka[16], F. Wäckerle[10], A. Wagner[27], C.P. Ward[5], D.R. Ward[5], J.J. Ward[15], P.M. Watkins[1], A.T. Watson[1], N.K. Watson[1], P.S. Wells[8], N. Wermes[3], J.S. White[28], B. Wilkens[10], G.W. Wilson[27], J.A. Wilson[1], G. Wolf[26], S. Wotton[5], T.R. Wyatt[16], S. Yamashita[24], G. Yekutieli[26], V. Zacek[18], D. Zer-Zion[8]

[1]School of Physics and Space Research, University of Birmingham, Birmingham B15 2TT, UK
[2]Dipartimento di Fisica dell' Università di Bologna and INFN, I-40126 Bologna, Italy
[3]Physikalisches Institut, Universität Bonn, D-53115 Bonn, Germany
[4]Department of Physics, University of California, Riverside CA 92521, USA
[5]Cavendish Laboratory, Cambridge CB3 0HE, UK
[6] Ottawa-Carleton Institute for Physics, Department of Physics, Carleton University, Ottawa, Ontario K1S 5B6, Canada
[7]Centre for Research in Particle Physics, Carleton University, Ottawa, Ontario K1S 5B6, Canada
[8]CERN, European Organisation for Particle Physics, CH-1211 Geneva 23, Switzerland
[9]Enrico Fermi Institute and Department of Physics, University of Chicago, Chicago IL 60637, USA
[10]Fakultät für Physik, Albert Ludwigs Universität, D-79104 Freiburg, Germany
[11]Physikalisches Institut, Universität Heidelberg, D-69120 Heidelberg, Germany
[12]Indiana University, Department of Physics, Swain Hall West 117, Bloomington IN 47405, USA
[13]Queen Mary and Westfield College, University of London, London E1 4NS, UK
[14]Technische Hochschule Aachen, III Physikalisches Institut, Sommerfeldstrasse 26-28, D-52056 Aachen, Germany
[15]University College London, London WC1E 6BT, UK
[16]Department of Physics, Schuster Laboratory, The University, Manchester M13 9PL, UK
[17]Department of Physics, University of Maryland, College Park, MD 20742, USA
[18]Laboratoire de Physique Nucléaire, Université de Montréal, Montréal, Quebec H3C 3J7, Canada
[19]University of Oregon, Department of Physics, Eugene OR 97403, USA
[20]Rutherford Appleton Laboratory, Chilton, Didcot, Oxfordshire OX11 0QX, UK
[21]CEA, DAPNIA/SPP, CE-Saclay, F-91191 Gif-sur-Yvette, France
[22]Department of Physics, Technion-Israel Institute of Technology, Haifa 32000, Israel
[23]Department of Physics and Astronomy, Tel Aviv University, Tel Aviv 69978, Israel
[24]International Centre for Elementary Particle Physics and Department of Physics, University of Tokyo, Tokyo 113, and Kobe University, Kobe 657, Japan
[25]Brunel University, Uxbridge, Middlesex UB8 3PH, UK
[26]Particle Physics Department, Weizmann Institute of Science, Rehovot 76100, Israel

[27]Universität Hamburg/DESY, II Institut für Experimental Physik, Notkestrasse 85, D-22607 Hamburg, Germany
[28]University of Victoria, Department of Physics, P O Box 3055, Victoria BC V8W 3P6, Canada
[29]University of British Columbia, Department of Physics, Vancouver BC V6T 1Z1, Canada
[30]University of Alberta, Department of Physics, Edmonton AB T6G 2J1, Canada
[31]Duke University, Dept of Physics, Durham, NC 27708-0305, USA
[32]Research Institute for Particle and Nuclear Physics, H-1525 Budapest, P O Box 49, Hungary
[33]Institute of Nuclear Research, H-4001 Debrecen, P O Box 51, Hungary
[34]Ludwigs-Maximilians-Universität München, Sektion Physik, Am Coulombwall 1, D-85748 Garching, Germany

[a] and at TRIUMF, Vancouver, Canada V6T 2A3
[b] and Royal Society University Research Fellow
[c] and Institute of Nuclear Research, Debrecen, Hungary
[d] and Department of Experimental Physics, Lajos Kossuth University, Debrecen, Hungary

1 Introduction

Relatively little attention has been paid so far to the spin properties of inclusively produced particles in parton hadronisation at LEP energies. The measurements which have been made of the polarisation of Λ and Λ_b hyperons [1] are essentially measurements of the polarisations of the primary s and b quarks from the Z^0 decay. Since in the static quark model the total spin of a Λ hyperon is assumed to be that carried by the heaviest of the valence quarks, these measurements relate primarily to the electroweak structure of the Z^0 production and decay, and only indirectly to the QCD aspects of the quark hadronisation.

For the $J^P = 1^-$ vector mesons however, which are $q\overline{q}$ systems of total spin one and orbital angular momentum zero, any alignment of the vector meson spin must arise at least in part from the hadronisation phase. In the commonly used Monte Carlo models of the hadronisation, such as the Lund string model [2] and the QCD cluster model [3], the spin aspects of particle production are essentially ignored. On the other hand, some predictions do exist [4–9] for the values of spin density matrix elements of inclusively produced vector mesons in e^+e^- annihilation. So far, only the B^* has been measured at LEP [10,11] and has been found to show no preferred spin alignment.

In this paper, measurements are reported of spin density matrix elements for three vector mesons produced in Z^0 decay at LEP: the $\phi(1020)$ which is studied at large scaled energy, $x_E > 0.7$, where it would be expected to contain a primary s or $\overline{s}$ quark (x_E is the ratio of the meson energy to the beam energy); $D^{*\pm}$ mesons which are studied over the range $x_E > 0.2$ and separated into components due to b quark production and direct c quark fragmentation; and a mixture of neutral and charged B^* mesons which arise from primary b quark fragmentation.

The paper starts with a discussion of the formalism of the spin density matrix and its relation to the angular distribution of meson decay products. Some theoretical motivation is then given, together with a summary of experimental results to date. After a brief description of the OPAL detector, the event and track selections are discussed. Then the measurements of the spin density matrix for the ϕ, D^* and B^* are covered in separate sections. Finally, the OPAL results are discussed in the light of previous measurements and theoretical models.

2 Vector meson angular decay distributions

The production and decay properties of particles possessing spin can be described in terms of a spin density matrix, $\rho_{mm'}$, where m and m' label the spin components along the quantization axis. The matrix $\rho_{mm'}$ is a 3×3 Hermitian matrix with unit trace whose diagonal elements ρ_{11}, ρ_{00} and ρ_{-1-1} are the relative intensities of meson spin components -1, 0 or $+1$. In the helicity basis, the matrix is usually called the helicity density matrix, and it is denoted $\rho_{\lambda\lambda'}$. The helicity $\lambda = \pm 1$ and $\lambda = 0$ states are sometimes called the transverse and longitudinal polarisation states. It should be noted that a mixture of states, such as for example one corresponding to $\rho_{11} = \rho_{-1-1} = 1/2$ and $\rho_{00} = 0$, with all off-diagonal elements equal to zero, is unpolarised in the conventional sense, although it is spin aligned. It is common to refer to $\rho_{00} = 1/3$ as describing a state of no spin alignment, regardless of the values of ρ_{11} and ρ_{-1-1} [4,12,13]. A detailed description of the formalism for production and decay of particles with spin may be found in [14].

Some or all of the elements of the spin density matrix can be measured using the angular distribution of the vector meson decay products, although for strong and electromagnetic decays, which conserve parity, it is not possible in the absence of interference effects to measure separately the values of ρ_{11} and ρ_{-1-1}. In the analysis described here, the density matrix elements are measured in the meson helicity rest frame, where the quantization axis (the z-axis) lies along the direction of motion of the meson in the overall centre-of-mass frame (the same as the laboratory frame at LEP). A common choice [14] of coordinates to define the azimuthal decay angle, $\phi_{\rm H}$, is to take the y-axis as the vector product of the direction of motion of the vector meson and the e^- beam direction (the helicity–beam frame). An alternative to the beam direction is to use the direction of motion of the outgoing quark or antiquark, which can be estimated from the event thrust axis; this gives the helicity–quark frame [4]. The formalism which follows is valid for any choice of frame.

For the decay of a vector meson to two pseudoscalars (e.g. $\phi \rightarrow$KK or $\mathrm{D}^* \rightarrow \mathrm{D}\pi$), the full angular distribution in the polar and azimuthal angles, $\theta_{\rm H}$ and $\phi_{\rm H}$, is given by:

$$\begin{aligned} W(\cos\theta_{\rm H},\phi_{\rm H}) &= \frac{3}{4\pi}\left[\frac{1}{2}(1-\rho_{00})+\frac{1}{2}(3\rho_{00}-1)\cos^2\theta_{\rm H}\right. \\ &\quad -\mathrm{Re}\,\rho_{1-1}\ \sin^2\theta_{\rm H}\cos 2\phi_{\rm H} - \frac{1}{\sqrt{2}}\mathrm{Re}\,(\rho_{10}-\rho_{0-1})\sin 2\theta_{\rm H}\cos\phi_{\rm H} \\ &\quad \left.+\mathrm{Im}\,\rho_{1-1}\ \sin^2\theta_{\rm H}\sin 2\phi_{\rm H} + \frac{1}{\sqrt{2}}\mathrm{Im}\,(\rho_{10}-\rho_{0-1})\sin 2\theta_{\rm H}\sin\phi_{\rm H}\right] \end{aligned} \quad (1)$$

which depends on five independent combinations of density matrix elements. After integration over $\phi_{\rm H}$ one has:

$$W(\cos\theta_{\rm H}) = \frac{3}{4}\ \left[(1-\rho_{00})+(3\rho_{00}-1)\cos^2\theta_{\rm H}\right]. \quad (2)$$

This distribution is isotropic for no spin alignment ($\rho_{00}=1/3$), and is proportional to $\sin^2\theta_{\rm H}$ for helicity ±1 states and to $\cos^2\theta_{\rm H}$ for helicity 0 states.

After integration over $\cos\theta_{\rm H}$ [15], the element ρ_{1-1} may be measured from:

$$W(|\alpha|) = (2/\pi)\ [1+2\,\mathrm{Re}\,\rho_{1-1}\cos 2|\alpha|\ ], \quad (3)$$

where $\alpha = |\phi_{\rm H}| - \pi/2$, and

$$W(|\beta|) = (2/\pi)\ [1+2\,\mathrm{Im}\,\rho_{1-1}\cos 2|\beta|\ ], \quad (4)$$

where $\beta = |\phi_{\rm H}+\pi/4| - \pi/2$.

Two asymmetries can be calculated [15] which depend on $\mathrm{Re}\,(\rho_{10}-\rho_{0-1})$ and $\mathrm{Im}\,(\rho_{10}-\rho_{0-1})$:

$$\mathrm{Re}\,(\rho_{10}-\rho_{0-1}) = -\frac{\pi}{2\sqrt{2}}\ \frac{N(\sin 2\theta_{\rm H}\cos\phi_{\rm H}>0)-N(\sin 2\theta_{\rm H}\cos\phi_{\rm H}<0)}{N(\sin 2\theta_{\rm H}\cos\phi_{\rm H}>0)+N(\sin 2\theta_{\rm H}\cos\phi_{\rm H}<0)}, \quad (5)$$

$$\mathrm{Im}\,(\rho_{10}-\rho_{0-1}) = \frac{\pi}{2\sqrt{2}}\ \frac{N(\sin 2\theta_{\rm H}\sin\phi_{\rm H}>0)-N(\sin 2\theta_{\rm H}\sin\phi_{\rm H}<0)}{N(\sin 2\theta_{\rm H}\sin\phi_{\rm H}>0)+N(\sin 2\theta_{\rm H}\sin\phi_{\rm H}<0)}, \quad (6)$$

where N corresponds to the number of events in the given angular range.

For the electromagnetic decay of a vector meson to a pseudoscalar plus vector, such as $\mathrm{B}^* \rightarrow \mathrm{B}\gamma$, the distribution, assuming imaginary parts of off-diagonal elements to be zero, is [8]:

$$\begin{aligned} W(\cos\theta_{\rm H},\phi_{\rm H}) &= \frac{1}{4\pi}\left[1-\frac{3\rho_{00}-1}{4}(3\cos^2\theta_{\rm H}-1)+\frac{3}{2}\mathrm{Re}\,\rho_{1-1}\ \sin^2\theta_{\rm H}\cos 2\phi_{\rm H}\right. \\ &\quad \left.+\frac{3\sqrt{2}}{2}\mathrm{Re}\,\rho_{10}\ \sin 2\theta_{\rm H}\cos\phi_{\rm H}\right] \end{aligned} \quad (7)$$

which may again be integrated over the polar or azimuthal angles. Thus, the distribution in the polar angle is:

$$W(\cos\theta_{\rm H}) = \frac{1}{2}\left[1 - \frac{3\rho_{00}-1}{4}(3\cos^2\theta_{\rm H} - 1)\right]. \quad (8)$$

The distribution in this case is proportional to $1+\cos^2\theta_{\rm H}$ for helicity ±1 states and to $\sin^2\theta_{\rm H}$ for helicity 0 states.

3 Models of vector meson production in hadronisation

In the present study, $\phi(1020)$ mesons are analysed at values of $x_E > 0.7$ where they may be expected (from the valence dominance hypothesis [16]) to contain a primary quark or antiquark from the Z^0 decay. In the case of the D^* mesons, the signal is separated into a component from decays of bottom hadrons and one coming from primary charm quarks. The latter type will contain a primary quark although some D^* mesons will be decay products of other charm hadrons. The B^* mesons will almost all contain a primary quark, although again some will be decay products.

A number of models place limits on the values of ρ_{00} in the helicity frame. Simple statistical models [4, 5] based on spin counting assume that the fragmentation process produces extra quark–antiquark pairs with all helicity states being equally probable. If the spin of the primary quark is parallel to that of the secondary antiquark, a vector meson is produced with helicity $\lambda = \pm1$. If the spins are antiparallel, either a pseudoscalar meson is produced with a probability f, or a vector meson with a probability $1-f$. In this model $\rho_{00} = (1-f)/(2-f)$, with a physical range of $0 < \rho_{00} < 0.5$ [4]. In terms of P/V, the ratio of pseudoscalar to vector meson production, the model gives $\rho_{00} = \frac{1}{2}(1-(P/V))$.

In a picture based on heavy quark effective theory [6], the light quarks in D^* and B^* mesons from heavy quark fragmentation are equally likely to be aligned along either direction relative to the fragmentation axis. This arises from parity conservation. In this theory $P/V = 1/3$, resulting in an expectation of $\rho_{00} = 1/3$.

A QCD-inspired model [7] describes the fragmentation process as the emission of soft gluons from the fast primary quark. These gluons decay into quark–antiquark pairs. At the end of the fragmentation chain one of the soft antiquarks combines with the fast quark to form a vector meson. The soft antiquark preferentially has the same helicity as the quark, corresponding to $\rho_{00} = 0$ for the vector meson.

Another model [4] describes the production of vector mesons through the channel $q \to qV$, with the vector meson coupling to the quark like a vector current. In this case, the helicity-conserving vector current ensures that the vector meson is always produced with $\lambda = 0$, corresponding to $\rho_{00} = 1$.

Some models make predictions about the behaviour of the off-diagonal elements of the spin density matrix [8, 9]. Non-zero off-diagonal elements may arise if the momentum of the meson is not parallel to that of the primary quark [17]. From the general properties of helicity amplitudes these elements are expected to be proportional to some power of $(p_{\rm T}/p)$, where $p_{\rm T}$ is the transverse momentum of the meson with respect to the primary quark and p is the meson momentum [4]. With typical values of $p_{\rm T} \sim 400$ MeV/c and the relatively large energies of the mesons in the present study, this contribution is expected to be small (< 0.02 for all

elements). In the incoherent class of models, where the fragmentation of the quark proceeds independently of the antiquark, the density matrices of the quark and antiquark are diagonal in the limit $p_T \to 0$ [8]. Off-diagonal elements generated by transverse momentum will then only be observable in frames referred to the internal properties of the jet, such as the helicity–quark frame. Values in the helicity–beam frame are expected to fall as a power of $\sqrt{s}$, and to be negligible at LEP energies [4].

Coherent models predict non-zero values for the off-diagonal elements even in the limit $p_T \to 0$. In the coherent approach, final-state interactions between the primary quark and antiquark are taken into account. For parity-conserving pure photon exchange ($\sqrt{s} \ll M_{Z^0}$), it has been shown [8] that the real component of the element ρ_{1-1} can be non-zero. Close to the Z^0 resonance ($\sqrt{s} \simeq M_{Z^0}$), the parity violating nature of the weak interaction also allows the imaginary component of ρ_{1-1} to be non-zero [9]. However, the imaginary component will be smaller than the real one by a factor of order 10^{-3} [9, 18]. (In the following analysis, the imaginary component of ρ_{1-1} is assumed to be zero for the D^*, but is measured for the ϕ as a check of procedures, and found to be zero). Off-diagonal elements generated by transverse momentum are expected to scale as a power of p_T/p as in the incoherent case, although it is an open question as to whether these elements should be observable in the helicity–beam frame or the helicity–quark frame.

4 Results from other experiments

A number of experiments have measured helicity matrix elements for $D^{*\pm}$ mesons produced in e^+e^- collisions at energies up to $\sqrt{s} = 29$ GeV [12, 13, 19]. The results are summarized in Table 1, where all results are determined in the helicity–beam frame. No strong evidence either for spin alignment ($\rho_{00} \neq 1/3$) or for coherence properties ($\rho_{\lambda\lambda'} \neq 0$ for $\lambda \neq \lambda'$) was found. In addition, results were presented in [12] for off-diagonal elements determined in the helicity–quark frame. These elements were found to be consistent with zero, although there was some indication that the magnitude of the elements increased with the transverse momentum of the D^* with respect to the jet. The spin alignment has also been measured for the production of $D^{*\pm}$ in collisions of a π^- beam with a fixed copper target [20]. The results were consistent with $\rho_{00} = 1/3$. Recently some measurements, also shown in Table 1, have been reported for B^* production at LEP, indicating no evidence for any spin alignment.

Other experiments have measured the density matrix for $\rho(770)^0$ mesons produced inclusively in deep inelastic electron [21] and neutrino [15, 22] scattering. Results from this class of experiment indicate that the $\rho(770)^0$ is produced with the helicity–zero state preferentially occupied.

5 The OPAL Detector

A complete description of the OPAL detector can be found in [23]. Tracking of charged particles is performed in a central detector, consisting of two layers of silicon microvertex detectors [24], a high-precision vertex drift chamber, a large-volume jet chamber, and a set of drift chambers

Reaction		Energy ($\sqrt{s}$)	Element	Result
$e^+ e^- \to D^{*\pm} X$	[13]	10.5 GeV	ρ_{00}	$0.36 \pm 0.01 \pm 0.01$
$e^+ e^- \to D^{*\pm} X$	[12]	29 GeV	ρ_{00}	0.37 ± 0.04
			Re ρ_{1-1}	0.04 ± 0.03
			Re ρ_{10}	0.00 ± 0.01
$e^+ e^- \to D^{*\pm} X$	[19]	29 GeV	ρ_{00}	$0.30 \pm 0.04 \pm 0.01$
			Re ρ_{1-1}	$0.01 \pm 0.03 \pm 0.00$
			Re ρ_{10}	$0.03 \pm 0.03 \pm 0.00$
$e^+ e^- \to B^* X$	[10]	M_{Z^0}	ρ_{00}	$0.32 \pm 0.04 \pm 0.03$
$e^+ e^- \to B^* X$	[11]	M_{Z^0}	ρ_{00}	$0.33 \pm 0.06 \pm 0.05$

Table 1: Measured values for elements of the helicity density matrix of $D^{*\pm}$ and B^* vector mesons from e^+e^- annihilation.

which measure the coordinates of tracks along the direction of the beam (z-chambers) [1]. The central detector is contained inside a solenoidal magnet producing a homogeneous axial field of 0.435 T. High precision reconstruction of secondary vertices is possible using the silicon microvertex detector, which covers polar angles $|\cos\theta| < 0.83$ with at least one layer of silicon detectors, or $|\cos\theta| < 0.77$ with two layers. Charged particle tracking is possible over nearly the full solid angle up to $|\cos\theta| = 0.98$. Particle identification for charged particles is performed using the specific energy loss, $\mathrm{d}E/\mathrm{d}x$, in the jet chamber [25].

The magnet coil is surrounded by a time-of-flight scintillator counter array and a lead glass electromagnetic calorimeter. A presampler is installed between these components which allows an improvement of the measurement of the longitudinal shower development and spatial resolution for showers which started in the magnet coil, and provides an additional space point on tracks leaving the central tracking system. The magnet return yoke is instrumented with nine layers of limited streamer tubes and serves as a hadron calorimeter. Outside the hadron calorimeter 93% of the solid angle is covered by at least 2 layers of muon chambers.

6 Event selection and Monte Carlo simulation

The analyses are based on about four million hadronic events collected with the OPAL detector on and around the Z^0 pole between 1990 and 1995. Hadronic Z^0 decays were selected using requirements on the number of reconstructed charged tracks and the energy deposited in the electromagnetic calorimeter. A detailed description of the criteria is given in [26]. For the D^* analysis, charged tracks and electromagnetic clusters unassociated to a charged track were combined into jets using the invariant mass algorithm with the E0 recombination scheme [27]. Within this algorithm, jets are defined by $x_{min} \equiv y_{cut} \cdot E_{vis}^2 = 49$ GeV^2, where E_{vis} is the total

[1] The OPAL coordinate system is defined with the z-axis following the electron beam direction. The polar angle θ is defined relative to this axis, and r and ϕ are the usual cylindrical polar coordinates.

visible energy and y_{cut} is defined in [27]. For the B^* analysis, jets were formed with charged tracks and unassociated electromagnetic clusters using a cone jet finding algorithm [28].

The events were divided into two hemispheres by the plane perpendicular to the direction of the thrust axis, calculated from charged tracks and neutral clusters unassociated to charged tracks. The primary vertex was reconstructed from the charged tracks, with the average beam position and the spread of the e^+e^- collision point used as an additional constraint.

To check analysis procedures and correct for detector inefficiencies and biases, 7 million hadronic decays of the Z^0 were simulated using the JETSET 7.4 Monte Carlo model [29] with parameters tuned to represent OPAL data [30]. No spin alignment was imposed on any particles, other than those which may arise naturally from certain decay chains (as discussed in Sect. 7.4); these are implemented by default in the program. For the ϕ analysis, 2 million of these events were used to evaluate the efficiency of the event selection. To enable precise efficiency corrections to be made for ϕ mesons at large momentum, a second sample of 40 000 events was produced containing ϕ mesons with generated scaled energy $x_E > 0.64$. This increased the Monte Carlo statistics for $\phi(1020)$ with measured $x_E > 0.7$ by a factor of about 14.5 with respect to the general purpose Monte Carlo sample. For the D^* analysis, a number of special samples were used to study specific decays, which corresponded to an additional 20 million hadronic Z^0 decays. In all samples heavy quark fragmentation was modelled following Peterson et al. [31]. All samples were passed through a detailed simulation of the OPAL detector [32] before being analysed with the same programs as for data.

7 The $\phi(1020)$ analysis

7.1 The ϕ event reconstruction and selection

The $\phi(1020)$ analysis used the data from the years up to 1994, giving a total of 3.5 million events. In each event, the cosine of the angle between the thrust and beam axes was required to be less than 0.9. The $\phi(1020)$ was reconstructed in its K^+K^- decay mode. The charged kaons were selected using the measured ionization energy loss (dE/dx) in the jet chamber with each track required to have at least 20 hits used for the measurement. A full description of the dE/dx measurement in OPAL can be found in [25]. The algorithm used for selecting charged kaons followed that of [33,34]. A χ^2 probability, or dE/dx weight, was calculated for four candidate particle types (electrons, pions, kaons and protons). The track was considered to be a kaon if the χ^2 probability was above 0.05 and was greater than those of the other particle hypotheses. Only ϕ mesons with $x_E > 0.7$ were considered for the analysis.

7.2 Measurement of the spin density matrix

The two-particle invariant masses and the decay angles $\cos\theta_H$ and ϕ_H were evaluated for all pairs of oppositely charged kaon candidates with total x_E greater than 0.7. To determine the

elements ρ_{00}, $\mathrm{Re}\,\rho_{1-1}$ and $\mathrm{Im}\,\rho_{1-1}$ the invariant masses were plotted in three equal bins of each of $|\cos\theta_{\mathrm{H}}|$, $|\alpha|$ and $|\beta|$ (as defined in Sect. 2).

The ϕ intensity in each bin was measured by fitting the mass spectra to the sum of a signal shape, taken from the Monte Carlo sample with the same cuts and particle identification as in the data, plus a quadratic function for the background. The fit was performed using a binned maximum-likelihood technique which correctly accounted for the finite Monte Carlo statistics [35], with the normalization of the background and the signal as free parameters. The fits for three bins of $|\cos\theta_{\mathrm{H}}|$ are shown in Fig. 1.

Corrections for detector effects, including geometrical acceptance, reconstruction efficiency and detector resolution were calculated from the Monte Carlo samples. The corrected differential rates in $|\cos\theta_{\mathrm{H}}|$, $|\alpha|$ and $|\beta|$ are shown in Fig. 2. All rates are corrected for the branching ratio to $\mathrm{K^+K^-}$, although the error on the branching ratio is not included since it is correlated over all bins. The data have been fitted to the appropriate angular distributions (equations 2, 3 and 4) with the relevant density matrix element and the normalization as free parameters. The elements $\mathrm{Re}\,(\rho_{10}-\rho_{0-1})$ and $\mathrm{Im}\,(\rho_{10}-\rho_{0-1})$ were calculated directly from the asymmetries (equations 5 and 6). The elements of the density matrix determined in this manner for all ϕ at $x_E > 0.7$ are summarized in Table 2.

7.3 Systematic errors

To calculate systematic errors on the ϕ density matrix elements, the following effects were studied:

- To determine systematic errors arising from the fitting of the mass spectra, two alternative parametrizations of the background were used, a Weibull Function [36] and the product of a linear function and an exponential. Fits were also performed with the mass range extended to 1.072 GeV. The fitted number of $\phi(1020)$ mesons per bin changed by up to 4%. However this shift was generally the same in all of the bins of a given angular distribution and so had only a small effect on the values of the density matrix elements. The maximum deviation on any of the five elements, 0.01, was taken as the systematic error for all elements.

- Because of bin migration effects arising from finite resolution, the detector corrections could bias [37] the corrected data distribution towards the original distribution in the Monte Carlo sample, which in this case is an isotropic decay distribution. Systematic effects also appear in the ϕ meson signal shapes used in the mass fits since, after detector effects, these depend on decay angles.

  To evaluate the magnitude of these effects, weights were applied to each $\phi(1020) \to \mathrm{K^+K^-}$ decay in the Monte Carlo sample according to the values of the decay angles before detector simulation. Five weights were applied, corresponding to the independent parameters in the decay angular distribution, equation 1. The weighted Monte Carlo could then be

used to form signal shapes for the fits to the mass spectrum and to calculate corrections for detector effects.

Each of the five weights was varied in turn within three standard deviations using the values of the matrix elements and their errors already determined. The full fitting and correction procedure was then performed again for each of the five matrix elements. A systematic error for each element was estimated by combining in quadrature the deviations from the value listed in Table 2 caused by varying each of the five weights. The errors on each element were found to be comparable and the largest estimate of 0.02 was assigned as the systematic error for all five elements.

- To account for differences between the fragmentation function in the data and the Monte Carlo sample, the $\phi(1020)$ rate was determined separately in the x_E ranges $0.7 < x_E < 0.754$, $0.754 < x_E < 0.827$ and $x_E > 0.827$. The ratios of the data to Monte Carlo rates were then used to weight the Monte Carlo according to the generator-level value of x_E. The determination of the spin density matrix was then repeated. The changes in the measurements of the density matrix elements were small, and the largest deviation, 0.01, was again taken as a conservative estimate of the systematic error on all elements.

- To evaluate any systematic errors due to differences in the treatment of $\mathrm{d}E/\mathrm{d}x$ in the data and Monte Carlo, the cut on the minimum number of $\mathrm{d}E/\mathrm{d}x$ hits on each track was increased from 20 to 40. The effect of changing this cut has some dependence on the angles θ_{H} and ϕ_{H}, while other possible systematic biases in $\mathrm{d}E/\mathrm{d}x$ would affect only the overall normalisation of the cross section. The change represented a $\sim$15% reduction in the reconstruction efficiency for high-x_E $\phi(1020)$ mesons. The determination of the spin density matrix was repeated and the elements of the density matrix were found to deviate on average by 0.04 from those listed in Table 2; this was assigned as the systematic error on all the elements.

- Small differences in tracking resolution between data and Monte Carlo, in both the track angle θ and the distance of closest approach to the vertex were accounted for by degrading the detector performance in the Monte Carlo. The determination of all spin density matrix elements was then repeated, and the typical shift was found to be 0.01.

A summary of the systematic errors is given in Table 3, and the final results for the spin density matrix in the helicity–beam frame are given in Table 2.

7.4 Contributions to $\phi(1020)$ production from particle decays

Spin-aligned, high-x_E $\phi(1020)$ mesons may arise from charmed particle decays of the type $\mathrm{P}_0 \to \mathrm{P}_1\phi(1020) \to \mathrm{P}_1\mathrm{K}^+\mathrm{K}^-$, where P_0 and P_1 are pseudoscalar mesons. In this case, the angular distribution of the ϕ decay products in the ϕ rest frame follows a $\cos^2\theta$ distribution with respect to the P_0 direction. This gives rise to a large value of ρ_{00} in the helicity frame. To understand the role of spin in the direct hadronisation process, the measured matrix elements have been

Element	All ϕ Helicity–beam frame	Primary ϕ Helicity–beam frame	$p_{\mathrm{T}} > 1.2$ GeV/c Helicity–quark frame
ρ_{00}	$0.54 \pm 0.06 \pm 0.05$	$0.53 \pm 0.06 \pm 0.05$	$0.56 \pm 0.09 \pm 0.05$
$\mathrm{Re}\,\rho_{1-1}$	$-0.11 \pm 0.05 \pm 0.05$	$-0.11 \pm 0.05 \pm 0.05$	$-0.12 \pm 0.14 \pm 0.05$
$\mathrm{Im}\,\rho_{1-1}$	$0.06 \pm 0.05 \pm 0.05$	$0.06 \pm 0.05 \pm 0.05$	$0.07 \pm 0.13 \pm 0.05$
$\mathrm{Re}\,(\rho_{10} - \rho_{0-1})$	$0.03 \pm 0.08 \pm 0.05$	$0.04 \pm 0.08 \pm 0.05$	$-0.12 \pm 0.17 \pm 0.05$
$\mathrm{Im}\,(\rho_{10} - \rho_{0-1})$	$-0.04 \pm 0.08 \pm 0.05$	$0.04 \pm 0.08 \pm 0.05$	$0.19 \pm 0.16 \pm 0.05$

Table 2: Measured helicity density matrix elements for ϕ mesons at $x_E > 0.7$. The first errors are statistical and the second systematic.

Source	Error
$\mathrm{d}E/\mathrm{d}x$ efficiencies	0.04
Bin migration	0.02
x_E distribution	0.01
Tracking	0.01
Fitting of mass distributions	0.01
Total	0.05

Table 3: Summary of systematic errors on the $\phi(1020)$ helicity density matrix elements.

corrected to take account of such decays, using the Monte Carlo simulation with measured charmed particle rates from data [38]. The dominant process is $\mathrm{D_s^{\pm}} \to \phi(1020)\pi^{\pm}$, while $\mathrm{D}^{\pm} \to \phi(1020)\pi^{\pm}$ and $\mathrm{D}^0 \to \phi(1020)\mathrm{K}^0$ also contribute. Table 2 gives the values for primary ϕ mesons, with statistical and systematic errors, after removal of these charm contributions (which account for only 5% of the total ϕ production at $x_E > 0.7$). The contribution from errors in the production rates of the charmed particles and their branching ratios to modes containing $\phi(1020)$ are much smaller than the systematic errors already present on the matrix elements.

7.5 Analysis in the helicity–quark frame

If hadronisation is described by independent fragmentation of partons, any correlation of the vector-meson production dynamics with the beam direction will be lost [4]. However, correlations may still exist with the direction of motion, directly after the decay of the Z^0, of the quark or antiquark initiating the jet containing the $\phi(1020)$. A more appropriate choice of the x–y plane is then that containing the momentum vectors of the quark and the vector meson, with the x-axis directed towards the quark (the helicity–quark frame). Off-diagonal helicity matrix elements generated by the transverse momentum of the vector meson with respect to

the original quark direction may be observable in this frame.

The initial direction of motion of the quark is estimated from the thrust axis, signed so that the angle between the high energy $\phi(1020)$ and the thrust axis is less than 90°. Monte Carlo studies show this to be a better estimate of the initial quark direction than the sphericity axis or the jet axis taken from jet-finding algorithms.

If the angle between the thrust axis and the vector meson direction is small, experimental errors make the x and y axes ill-defined. For this reason, a cut was imposed on the transverse momentum of the ϕ with respect to the thrust axis, $p_{\mathrm{T}} > 1.2$ GeV/c. The resolution on the azimuthal angle ϕ_{H} in the helicity–quark frame is nevertheless still poorer than in the helicity–beam frame, increasing the significance of bin migration effects.

The increase in the importance of bin-migration effects means that the results are sensitive to the angular distributions in the Monte Carlo sample used to correct the data. To account for this, an iterative procedure was adopted. Each element of the density matrix in turn was first determined as before using correction factors taken from the unweighted Monte Carlo sample. The result was then used to weight the Monte Carlo distribution at the generator level towards the measured data distribution, yielding new correction factors which were applied to the data. New fits were then made to the data and the procedure was iterated until the measurements converged, defined as being when the change in the data value was less than 10% of the statistical error.

The statistical errors were corrected in a similar fashion. The above determination of the matrix element yields a value and associated one standard deviation error. The value at the upper error limit was then used to weight the Monte Carlo, obtaining a new estimate of the upper error limit. Again, the procedure was iterated until the estimate of the upper error limit converged. The procedure was repeated for the lower error limit.

The resulting values of the spin density matrix elements are given in the final column of Table 2. There is no indication, within rather large errors, of non-zero values for off-diagonal elements. The element ρ_{00} is compatible with that measured for the full data sample, suggesting that ρ_{00} does not depend significantly on p_{T}.

8 The D* analysis

8.1 The D* event selection

In the D* analysis, which used all the data for the years 1990 to 1995, the following decay chain and its charge conjugate were searched for:

$$\begin{aligned} \mathrm{D}^{*+} &\rightarrow \mathrm{D}^0 \pi_{\mathrm{s}}^+ \\ &\quad\hookrightarrow \mathrm{K}^- \pi^+ \ , \end{aligned}$$

where π_{s} denotes a slow, low-momentum pion. The track quality cuts, as well as the method of reconstructing the D* candidates, and the selection cuts applied to these, have been described

in previous OPAL publications [39,40]. Candidates were selected by using all combinations of tracks which passed the track quality cuts. Two oppositely charged tracks were combined for the D^0 candidate, with one of them assumed to be a kaon and the other a pion. To form the D^* candidate, a third track was added as the slow pion if its charge was the same as that of the assumed pion in the D^0 decay. The candidates were required to lie in the the mass range, 1790 MeV/c^2 $< M_{D^0}^{\rm cand} <$ 1940 MeV/c^2, and only those combinations with $x_E > 0.2$ were used in the analysis. The D^* signal was identified as the expected peak at about 145 MeV/c^2 in the spectrum of the mass difference $\Delta M = M_{D^*}^{\rm cand} - M_{D^0}^{\rm cand}$.

8.2 Determination of the background fraction

The data were used to determine the background in the mass difference spectrum. Three event samples were used:

- **wrong-charge candidates** were selected by requiring that the charges of both tracks of the D^0 candidate decay products be equal, and the charge of the slow pion candidate track be of opposite sign;
- **reflected pion candidates** were constructed by selecting a slow pion candidate track from the hemisphere opposite to a normal D^0 candidate and adding it to the event after reflecting it about the origin;
- **reflected pion wrong-charge candidates** required both a wrong-charge D^0 candidate and a reflected pion.

These samples were added together and their mass difference ΔM distribution was normalized to the D^* candidate distribution in the sideband region 160 MeV/c^2 $< \Delta M <$ 200 MeV/c^2. The ΔM distribution for D^* candidates with the background superimposed is shown in Fig. 3. The number of candidate and background events was determined in bins of x_E by counting the entries in a ΔM window, 142 MeV/c^2 $< \Delta M <$ 149 MeV/c^2, in both the candidate and background distributions. The number of D^* mesons was obtained by subtracting one from the other. The numbers and the background fractions, $f_{\rm bgd} = N_i^{\rm bgd}/N_i^{\rm cand}$, are given in Table 4. This procedure, when applied to the Monte Carlo, reproduces well the true background. The final number of background-subtracted D^* candidates was 5959 ± 104.

8.3 Separation method for b $\rightarrow$ D^* and c $\rightarrow$ D^*

Nearly all D^* mesons are produced in bottom and charm decays. An analysis attempting to study properties of the charm quark therefore has to separate these components. The flavour separation method described below uses bottom and charm fractions as a function of scaled energy x_E, combined with lifetime information, in order to calculate event probability weights. These probabilities were then used in the fits to obtain the helicity matrix element ρ_{00}.

x_E	$N_{\rm cand}$	$N_{\rm bgd}$	$N_{\rm D^*}$	$f_{\rm bgd}$
0.2-0.3	3271	1911 $\pm$ 27	1360 $\pm$ 63	0.584 $\pm$ 0.013
0.3-0.4	1960	792 $\pm$ 17	1168 $\pm$ 48	0.404 $\pm$ 0.013
0.4-0.5	1322	301 $\pm$ 11	1021 $\pm$ 38	0.228 $\pm$ 0.010
0.5-0.6	1363	329 $\pm$ 11	1034 $\pm$ 39	0.241 $\pm$ 0.010
0.6-0.7	855	146 $\pm$ 7	709 $\pm$ 30	0.171 $\pm$ 0.010
0.7-0.8	501	56 $\pm$ 4	446 $\pm$ 23	0.112 $\pm$ 0.010
0.8-0.9	213	19 $\pm$ 2	194 $\pm$ 15	0.089 $\pm$ 0.012
0.9-1.0	31	3 $\pm$ 1	28 $\pm$ 6	0.097 $\pm$ 0.030

Table 4: Number of $\rm D^*$ candidates ($N_{\rm cand}$) reconstructed as a function of x_E, together with the background ($N_{\rm bgd}$) and the background subtracted numbers ($N_{\rm D^*}$). The error quoted for the number of $\rm D^*$ mesons is the total statistical error of the sample, $\sqrt{N_{\rm cand} + \sigma^2_{N_{\rm bgd}}}$. The errors on the background and $f_{\rm bgd}$ are statistical only.

The fractions of $\rm c \to D^*$ and $\rm b \to D^*$ were determined in a previous OPAL publication [40], as a function of x_E. There, the decays of charm quarks were separated from those of bottom quarks by a combination of b-tagging methods using leptons, jet shape variables, and lifetime information, in a fragmentation function independent analysis. The b fractions, $f_{\rm b}(x_E)$, are listed in Table 5.

x_E	$f_{\rm b} \pm \sigma_{\rm stat} \pm \sigma_{\rm sys}$
0.2-0.3	0.705$\pm$0.053$\pm$0.056
0.3-0.4	0.796$\pm$0.056$\pm$0.053
0.4-0.5	0.623$\pm$0.055$\pm$0.045
0.5-0.6	0.316$\pm$0.053$\pm$0.039
0.6-0.7	0.143$\pm$0.052$\pm$0.043
0.7-0.8	0.005$\pm$0.047$\pm$0.049
0.8-0.9	0.058$\pm$0.080$\pm$0.044
0.9-1.0	0.340$\pm$0.260$\pm$0.059

Table 5: Bottom fractions per x_E bin, with their statistical and systematic errors [40].

The lifetime information for the weight calculation was evaluated using decay length significance distributions. For each jet in the event, a secondary vertex was reconstructed by an iterative procedure. A decay length was calculated between this vertex and the primary vertex in the event, in a plane perpendicular to the beam direction. The decay length significance was calculated for the $\rm D^*$ jet, $d/{\sigma_d}^{\rm s}$, and for the highest energy jet not containing the $\rm D^*$, $d/{\sigma_d}^{\rm o}$. The event-by-event weights for the signal and background were determined using $d/{\sigma_d}^{\rm s}$, while

the charm and bottom weights were calculated using $d/\sigma_d{}^\circ$. In this case, the jet containing the D^* candidate was not used because lifetime information in this jet is sensitive to the time dependent mixing in the B system. The measurement of the decay length significance, $d/\sigma \equiv \delta$, in a specific event was compared to the expected distributions for signal, background, bottom and charm events, and a probability for this measurement was calculated. This method has been described in detail in [39].

As far as possible, real data were used to calculate the probabilities. The functions $L(\delta_i|x_i)$ were used, which are the probability density functions of the decay length significances, where x_i is the scaled energy (x_E) of the candidate. The distributions for all candidates, $L_{\rm cand}(\delta|x)$, and for background events, $L_{\rm bgd}(\delta|x)$ were taken directly from the data sample distributions. The background distributions were estimated from the reflected candidates found in the ΔM region, 140 MeV/c^2 $< \Delta M <$ 200 MeV/c^2. The weights for an event to be signal or background were calculated using:

$$w_{\rm sig}(\delta_i|x_i) \;=\; \frac{L_{\rm cand}(\delta_i|x_i) - f_{\rm bgd}(x_i)\cdot L_{\rm bgd}(\delta_i|x_i)}{L_{\rm cand}(\delta_i|x_i)} = 1 - w_{\rm bgd}(\delta_i|x_i)\ . \tag{9}$$

The fractions $f_{\rm bgd}(x)$ are taken from Table 4.

Monte Carlo simulation was used to predict the equivalent distributions for bottom and charm events, $L_{\rm c}(\delta)$ and $L_{\rm b}(\delta)$. These are the probability density functions for the highest energy jet not containing the D^*. It was assumed that the lifetime information in this jet was unbiased with respect to the D^* momentum. Samples of approximately 100 000 $b\bar{b} \to D^*$ and 100 000 $c\bar{c} \to D^*$ Monte Carlo events were used in the selected channel. The weights are given by:

$$w_{\rm b}(\delta_i|x_i) \;=\; \frac{f_{\rm b}(x_i)L_{\rm b}(\delta_i)}{f_{\rm b}(x_i)L_{\rm b}(\delta_i) + f_{\rm c}(x_i)L_{\rm c}(\delta_i)} = 1 - w_{\rm c}(\delta_i|x_i)\ . \tag{10}$$

The quantities $f_{\rm b}(x_i)$ and $f_{\rm c}(x_i)(= 1 - f_{\rm b}(x_i))$ are the fractions of bottom and charm events in the sample, taken from Table 5.

8.4 Measurement of ρ_{00}

The measurement of the spin alignment was done in terms of the parameter ζ defined by $\zeta = (3\rho_{00} - 1)/(1 - \rho_{00})$, which was extracted from the data using an unbinned log-likelihood fit. Since it is possible that $b \to D^*$ and background events may produce structure in the $\cos\theta_{\rm H}$ distribution, it was necessary to separate the flavour components. The technique and the likelihood function are described in the first part of this section. The fit and its results are discussed in the second part.

The angle $\theta_{\rm H}$, which is the angle of the slow pion in the D^* rest frame, is measured with respect to the D^* direction in the laboratory. The logarithm of the likelihood function is a sum which runs over all candidates i considered:

$$\log \mathcal{L} = \sum_i \log\ (\mathcal{L}_i/\mathcal{N}_i)\ , \tag{11}$$

where $\mathcal{N}_i$ is the likelihood normalization calculated for each event. The observed spin alignment parameter has contributions from bottom, charm and background events, and the likelihood function is parametrized following equation 2:

$$\mathcal{L}_i \;=\; \left\{1 + \left[w^i_{\rm sig}(w^i_{\rm b}\zeta_{\rm b} + w^i_{\rm c}\zeta_{\rm c}) + w^i_{\rm bgd}\zeta_{\rm bgd}\right]\cos^2\theta^i_{\rm H}\right\}\ , \tag{12}$$

where the w^i are the individual event weights for a $\rm D^*$ meson to originate from the source indicated, and $\zeta_{\rm c}$, $\zeta_{\rm b}$ and $\zeta_{\rm bgd}$ are the free parameters in the fit. Because of limited statistics, the ζ parameters were taken to be independent of x_E. The normalization $\mathcal{N}_i$ is obtained by integrating $\mathcal{L}_i$ with respect to $\cos\theta^i_{\rm H}$ over the whole range of values, from -1 to $+1$: $\mathcal{N}_i = 2\{1 + [w^i_{\rm sig}(w^i_{\rm b}\zeta_{\rm b} + w^i_{\rm c}\zeta_{\rm c}) + w^i_{\rm bgd}\zeta_{\rm bgd}]/3\}$. Monte Carlo studies have shown that the efficiencies have no significant dependence on $\cos\theta_{\rm H}$ since the momentum of the slow pion in the $\rm D^*$ rest frame is sufficiently small that its laboratory momentum is relatively insensitive to the decay angle.

In addition to the $\rm D^*$ candidate events entering the fit, wrong-charge events which passed all the $\rm D^*$ selection cuts and were found within the ΔM window were used to improve the fitting of the background component. Monte Carlo studies have shown that these events simulate well the spin alignment of the background. Fitting only these background events yielded a spin alignment parameter of $\zeta_{\rm bgd} = -0.02 \pm 0.05$ (stat), which is consistent with zero.

The data were fitted to extract simultaneously values of $\zeta_{\rm c}$, $\zeta_{\rm b}$ and $\zeta_{\rm bgd}$, with the results:

$$\begin{aligned} \zeta_{\rm c} &= 0.31 \pm 0.11 \\ \zeta_{\rm b} &= 0.02 \pm 0.12 \\ \zeta_{\rm bgd} &= -0.04 \pm 0.05\ , \end{aligned}$$

where the error quoted is statistical. The fit was found to be stable as the initial input ζ values and the step sizes were varied. The likelihood function was scanned for the 3 parameters, and clear well-behaved minima were obtained. The value of $\zeta_{\rm c}$ translates into a value for $\rho^{\rm c}_{00} = (1 + \zeta_{\rm c})/(3 + \zeta_{\rm c})$ of:

$$\rho^{\rm c}_{00} = 0.40 \pm 0.02\ ,$$

where the superscript on $\rho^{\rm c}_{00}$ indicates that this result is for the charm component of the sample. In Fig. 4 the $\rm D^*$ candidate $\cos\theta_{\rm H}$ distribution is shown. The result of the 3-parameter log-likelihood fit is superimposed (and should not be confused with a direct fit to the distribution).

8.5 Measurement of Reρ_{1-1}

The real component of the off-diagonal element ρ_{1-1} is expected to be an order of magnitude smaller than ρ_{00}. The imaginary component is assumed to be negligible with respect to the real component, as discussed in Sect. 3 and confirmed for the ϕ meson by the measurements. A non-zero value of the real component would be a clear indication of final-state interactions between the primary quark and antiquark, also known as coherence effects [8]. As discussed in

Sect. 2 this element can be measured by studying the azimuthal distribution of the π_s in a plane perpendicular to the D^* direction, with respect to a reference axis. The angle $\alpha = |\phi_H| - \pi/2$ in the helicity–beam frame (see Sect. 2) was measured in this analysis.

The expected angular distribution is given by equation 3. Since the value of $\mathrm{Re}\,\rho_{1-1}$ is expected to be small, a fit to the $|\alpha|$ distribution was performed, as in the ϕ analysis, rather than using the full likelihood fit. The D^* candidates with $x_E > 0.5$ were used, thus increasing the charm purity of the sample to $81 \pm 4\%$, and the $|\alpha|$ distribution was fitted over the range 0 to $\pi/2$ to the expected angular distribution. A fit was also performed to the background-subtracted sample, where the background was determined as described in Sect. 8.2.

The background events were fitted separately in a log-likelihood fit similar to the one performed for the ρ_{00} analysis, for both data and Monte Carlo. The fit results, $\mathrm{Re}\,\rho_{1-1}^{\mathrm{bgd}}(\mathrm{data}) = -0.009 \pm 0.012$ and $\mathrm{Re}\,\rho_{1-1}^{\mathrm{bgd}}(\mathrm{MC}) = 0.010 \pm 0.011$ are consistent with a zero value for $\mathrm{Re}\,\rho_{1-1}$.

For the background-subtracted D^* candidates, the fit to the Monte Carlo events, where a null value is expected, gave $\mathrm{Re}\,\rho_{1-1}^{\mathrm{MC}} = -0.003 \pm 0.011$. For the data, $\mathrm{Re}\,\rho_{1-1}$ was measured to be:

$$\mathrm{Re}\,\rho_{1-1} \;=\; -0.039 \pm 0.014 \;,$$

where the error quoted is statistical. The fit to the background-subtracted data is shown in Fig. 5.

8.6 Systematic errors

The set of systematic errors which are specifically related to the log-likelihood fit discussed previously only apply to the ζ_c measurement associated to ρ_{00}^c. The error related to the background determination applies to both the $\mathrm{Re}\,\rho_{1-1}$ and ρ_{00}^c measurements. The following sources were considered:

- The background was estimated using the technique described in Sect. 8.2. The systematic error of this method was evaluated using the full Monte Carlo sample of events, by comparing the true background to the estimated background. In the case of the ρ_{00}^c measurement, this affects the calculation of the weights entering the log-likelihood fit. In the $\mathrm{Re}\,\rho_{1-1}$ case, it affects the background subtraction.

- The $f_b(x_E)$ fractions were varied within their statistical and systematic errors, and the differences in the result of the fit were used to estimate the systematic errors on ζ_c, ζ_b and ζ_{bgd}.

- The background fractions $f_{\mathrm{bgd}}(x_E)$ were varied within their errors to determine the systematic error on the fitted ζ.

- The bottom and charm weights were determined with a limited number of Monte Carlo events; the associated statistical error was taken into account.

- The B^0 lifetime has been measured precisely: $\tau_{B^0} = 1.57 \pm 0.08$ ps [41]. The $b\bar{b} \to D^*$ Monte Carlo events used to determine the bottom weights w_b were reweighted within the limits of the measured B lifetime, and the fit was repeated with these new weights.

- The bottom and charm Monte Carlo events were generated with a Peterson fragmentation function, using the parameters, $\epsilon_c = 0.046$ and $\epsilon_b = 0.0057$, corresponding to mean scaled energies $< x_E >$ of 0.508 and 0.700 respectively. The Monte Carlo events were reweighted within the limits, $0.0038 < \epsilon_b < 0.0085$ [42] and $0.03 < \epsilon_c < 0.07$, as experimentally measured [43,44]. The different sets of weights were then used to recalculate the fitted ζ values.

- Approximately 22% of the data events do not contain track information from the silicon microvertex detector. This ratio must be reproduced in the bottom and charm Monte Carlo samples used to calculate the w_c and w_b weights. In effect, the decay length significance distributions are sensitive to the merging efficiencies for track reconstruction. The Monte Carlo samples were reweighted for this ratio of non-silicon to silicon events, and the fit was performed with the flavour separation weights determined using these reweighted Monte Carlo samples.

- It has been observed that the fit systematically underestimates ζ_c by approximately 10%, although the effect on the final ρ^c_{00} value is small. This shift is present in Monte Carlo studies, and it is believed to originate from the lack of statistics. These studies show that the size of the bias depends on the number of events in the sample. This was applied as a correction to the fitted value of ζ_c. The full systematic shift was also taken as the systematic error.

A list of all systematic errors is given in Table 6.

Systematic error source	$\Delta(\zeta_c)$	$\Delta(\zeta_b)$	$\Delta(\zeta_{bgd})$	$\Delta(\rho^c_{00})$	$\Delta(\mathrm{Re}\,\rho_{1-1})$
Background determination	0.013	0.018	0.001	0.003	0.007
Error on f_b fraction	0.027	0.014	0.001	0.005	-
Error on f_{bgd}	0.031	0.010	0.001	0.006	-
Monte Carlo statistics	0.001	0.013	0.001	0.000	-
B lifetime	0.004	0.006	0.001	0.001	-
Heavy flavour fragmentation	0.016	0.013	0.004	0.003	-
Merging efficiency	0.002	0.005	0.001	0.000	-
Fit systematics	0.029	0.024	0.002	0.006	-
Total	0.055	0.040	0.005	0.011	0.007

Table 6: List of the systematic errors in the D^* analysis for the ζ parameters, ρ^c_{00} and $\mathrm{Re}\,\rho_{1-1}$.

8.7 Summary of D* results

The spin density matrix elements ρ_{00} and $\mathrm{Re}\,\rho_{1-1}$ were measured for D^* mesons using 5959 ± 104 $\mathrm{D}^{*\pm}$ candidate events. In the $\mathrm{Re}\,\rho_{1-1}$ case, only candidates with $x_E > 0.5$ were considered. The results are:

$$\begin{aligned} \rho_{00}^{\mathrm{c}} &= 0.40 \pm 0.02 \pm 0.01 \\ \mathrm{Re}\,\rho_{1-1} &= -0.039 \pm 0.014 \pm 0.007 \end{aligned}$$

where the errors are statistical and systematic. The ρ_{00} matrix element was evaluated in a three parameter fit, separately for $\mathrm{c} \to \mathrm{D}^*$, $\mathrm{b} \to \mathrm{D}^*$ and background events, and ρ_{00}^{c} is the value obtained specifically for the charm component of the sample. This includes both directly produced D^* mesons and those from excited charm hadron decays.

9 The B* analysis

Full details of the study of B^* meson production in OPAL have recently been reported elsewhere [45]; there the spin alignment result is presented in terms of relative contributions of transverse and longitudinal polarisation states and is compared to similar measurements by other LEP experiments. In the present paper, the measurement is discussed using the formalism of the helicity density matrix, and is compared to the results obtained for the ϕ and D^* mesons.

From the sample of 4.1 million events taken during 1991-95, a total of 1894 B^* meson candidates were reconstructed in the decay $\mathrm{B}^* \to \mathrm{B}\gamma$. The B mesons were reconstructed inclusively in jets containing a secondary vertex, reconstructed as described in [46]. The energy of the B meson was estimated by using the weighted sum of the momenta of charged particles associated to the secondary vertex, where the weights were functions of the track momenta and impact parameters with respect to the primary and secondary vertices. Unassociated energy in the electromagnetic calorimeters was added, after scaling, if it lay within a narrow cone about an initial proposed B direction determined using the charged tracks. The B direction was then estimated using the azimuthal angle of the direction from the primary to the secondary vertex, and the polar angle of the vector sum of the track and electromagnetic cluster momenta assigned to the B. The sample thus obtained included charged and neutral B meson candidates.

The photons from B^* decay, which have laboratory momentum below 800 MeV/c, were identified by their conversion in the material of the OPAL detector. Such photons, consistent with coming from the primary vertex, were combined with all B candidates in the same event hemisphere as defined using the thrust axis. The B^* signal was then identified using the expected peak in the distribution of mass difference between the B^* and B candidate track combinations.

The efficiency to detect conversion photons is sufficiently high above a laboratory energy of about 300 MeV to allow their polar angle distribution in the B^* rest frame to be measured over the range $\cos\theta_{\mathrm{H}} > -0.4$. The B^* candidates were divided up into bins of $\cos\theta_{\mathrm{H}}$ and the

contribution in each bin was obtained by fitting the B^*–B mass difference distribution. The result is shown in Fig. 6 together with a curve from a least squares fit to the form of equation 8. The ρ_{00} matrix element evaluated for the B^* is:

$$\rho_{00} = 0.36 \pm 0.06 \pm 0.07 \ ,$$

where the first error is statistical and the second systematic. The result is consistent with no spin alignment.

The principal sources of systematic error on this measurement arose from the photon acceptance correction, which was a strong function of $\cos\theta_{\rm H}$, and from the background subtraction procedure. A full discussion of these effects is given in [45].

10 Summary and conclusions

In an analysis of inclusive vector meson production in Z^0 decay using the OPAL data, measurements have been made for some helicity density matrix elements for $\phi(1020)$ at high x_E, for $D^{*\pm}$ and for B^* mesons. The diagonal elements were measured to be:

$$\begin{aligned}
&\rho_{00} = 0.54 \pm 0.06 \pm 0.05 \quad \text{for } \phi(1020) \text{ at } x_E > 0.7 \\
&\rho_{00} = 0.40 \pm 0.02 \pm 0.01 \quad \text{for } D^* \text{ mesons from c fragmentation} \\
&\rho_{00} = 0.36 \pm 0.06 \pm 0.07 \quad \text{for a mixture of charged and neutral } B^* \text{ mesons}
\end{aligned}$$

In the helicity–beam frame, off-diagonal elements were measured as:

$$\begin{aligned}
{\rm Re}\,\rho_{1-1} &= -0.11 \pm 0.05 \pm 0.05 \quad \text{for } \phi(1020) \text{ at } x_E > 0.7 \\
{\rm Re}\,\rho_{1-1} &= -0.039 \pm 0.014 \pm 0.007 \quad \text{for } D^* \text{ mesons with } x_E > 0.5
\end{aligned}$$

The results indicate that $\phi(1020)$ mesons containing the primary (anti)quark from the decay of the Z^0 are produced with unequal populations of the three helicity states. The value of $\rho_{00} = 0.54 \pm 0.06 \pm 0.05$ indicates that the helicity zero state is preferentially occupied. This result could be consistent with models based on simple spin-counting arguments (which require $\rho_{00} \leq 1/2$) although it would require rather a large suppression of pseudoscalar meson production in the hadronisation. The result is in agreement with models where the $\phi(1020)$ couples to the primary quark like a vector current.

The D^* also has $\rho_{00} > 1/3$, although the value is not as large as that for the $\phi(1020)$. However, the result may be taken as a lower limit for direct D^* production since decays of orbitally excited D^{**} mesons [47] may dilute any spin alignment in the D^* signal. In the statistical picture, $\rho_{00} > 1/3$ would imply a vector to pseudoscalar ratio larger than 3; in fact, the available measurements [48] tend to favour a value lower than 3. This suggests that some other mechanism is responsible for the observed spin alignment.

The results for B^* production agree with the other measurements at LEP, indicating no evidence for spin alignment of the B^* mesons. The absence of alignment is consistent with

the simple statistical picture where the primary b quark hadronises to produce vector and pseudoscalar mesons in the ratio of 3:1, as indeed is observed in the LEP experiments [10,11,45]. However, as with the D^*, approximately 20% of the B^* mesons may be decay products of the orbitally excited B^{**} states [49], and so some alignment of the primary contribution is not ruled out.

Off-diagonal elements of the spin density matrix have been determined for both the ϕ and the D^* in the frame where the x–y plane is defined using the beam axis (the helicity–beam frame). All measured elements are compatible with zero, with the exception of the element $\mathrm{Re}\,\rho_{1-1}$ for the D^* which shows a small difference from zero. Such a result is expected from coherence (non-independent fragmentation) in the production process. For the ϕ mesons the off-diagonal elements in the helicity–quark frame are compatible with zero, although they have large statistical errors due to the uncertainty in the original quark direction.

The measurements reported here show some evidence that spin plays a role in the production dynamics of vector mesons from parton hadronisation at LEP energies. In most cases however, the deviations from isotropy in the decay distributions are small, and similar measurements of other vector mesons, such as ρ^0, ω, $K^{*\pm}$, K^{*0} and D^{*0} would clearly be useful in improving the theoretical understanding of the role of spin in hadronisation.

Acknowledgements

We particularly wish to thank the SL Division for the efficient operation of the LEP accelerator and for their continuing close cooperation with our experimental group. In addition to the support staff at our own institutions we are pleased to acknowledge the
Department of Energy, USA,
National Science Foundation, USA,
Particle Physics and Astronomy Research Council, UK,
Natural Sciences and Engineering Research Council, Canada,
Israel Science Foundation, administered by the Israel Academy of Science and Humanities,
Minerva Gesellschaft,
Japanese Ministry of Education, Science and Culture (the Monbusho) and a grant under the Monbusho International Science Research Program,
German Israeli Bi-national Science Foundation (GIF),
Direction des Sciences de la Matière du Commissariat à l'Energie Atomique, France,
Bundesministerium für Bildung, Wissenschaft, Forschung und Technologie, Germany,
National Research Council of Canada,
Avadh Bhatia Foundation, University of Alberta, Canada,
Hungarian Foundation for Scientific Research, OTKA T-016660, and OTKA F-015089.

We also wish to thank Prof M. Anselmino for illuminating discussions and suggestions which greatly aided our analyses.

References

[1] ALEPH Coll., D. Buskulic et al.: Phys. Lett. B357 (1996) 437;
ALEPH Coll., D. Buskulic et al.: Phys. Lett. B374 (1996) 319

[2] B. Andersson, G. Gustafson, G. Ingelman and T. Sjöstrand: Phys. Rep. 97 (1983) 31

[3] G. Marchesini et al.: Comp. Phys. Commun. 67 (1992) 465

[4] J.F. Donoghue: Phys. Rev. D19 (1979) 2806

[5] I.I.Y. Bigi: Nuovo Cimento A41 (1977) 581

[6] A.F. Falk and M.E. Peskin: Phys. Rev. D49 (1994) 3320

[7] J.E. Augustin and F.M. Renard: in M. Jacob (Ed.), *Proc. LEP Summer Study (1978, Les Houches and CERN)*, Vol. 1, CERN 79-01, p 185

[8] M. Anselmino, P. Kroll and B. Pire: Z. Phys. C29 (1985) 135

[9] A. Anslem, M. Anselmino, F. Murgia and M.G. Ryskin: J. Exp. Th. Phys. 60 (1994) 496

[10] DELPHI Coll., P. Abreu et al.: Z. Phys. C68 (1995) 353

[11] ALEPH Coll., D. Buskulic et al.: Z. Phys. C69 (1995) 393

[12] HRS Coll., S. Abachi et al.: Phys. Lett. B199 (1987) 585

[13] CLEO Coll., Y. Kubota et al.: Phys. Rev. D44 (1991) 593

[14] C. Bourrely, E. Leader and J. Soffer: Phys. Rep. 59 (1980) 95

[15] BBCN Coll., V.G. Yatez et al.: Z. Phys. C66 (1995) 583

[16] P. Nason and B.R. Webber: Phys. Lett. B33 (1994) 405

[17] J.F. Nieves: Phys. Rev. D20 (1979) 2775

[18] M. Anselmino: private communication.

[19] TPC–Two-Gamma Coll., H. Aihara et al.: Phys. Rev. D43 (1991) 29

[20] K. Rybicki and R. Rylko: Acta Phys. Pol. B24 (1993) 1049

[21] I. Cohen et al.: Phys. Rev. D25 (1982) 634

[22] BEBC WA59 Coll., W. Wittek et al.: Phys. Lett. B187 (1987) 179

[23] OPAL Coll., K. Ahmet et al.: Nucl. Instrum. Methods A305 (1991) 275

[24] P.P. Allport et al.: Nucl. Instrum. Methods A324 (1993) 34;
P.P. Allport et al.: Nucl. Instrum. Methods A346 (1994) 476

[25] M. Hauschild et al.: Nucl. Instrum. Methods A314 (1992) 74

[26] OPAL Coll., G. Alexander et al.: Z. Phys. C5 (1991) 175

[27] JADE Coll., W. Bartel et al.: Z. Phys. C33 (1986) 23;
JADE Coll., S. Bethke et al.: Phys. Lett B213 (1988) 235

[28] OPAL Coll., R. Akers et al.: Z. Phys. C63 (1994) 197
The maximum half-angle of the cone was set to 0.65 radians.

[29] T. Sjöstrand, Comp. Phys. Commun 39 (1986) 347;
T. Sjöstrand and M. Bengtsson, Comp. Phys. Commun 43 (1987) 367;
T. Sjöstrand, CERN manual CERN-TH.7112/93 (1993) (Geneva, CERN)

[30] OPAL Coll., M.Z. Akrawy et al.: Z. Phys. C47 (1990) 505;
The JETSET 7.4 parameters were tuned as described in OPAL Coll., G. Alexander et al.: Z. Phys. C69 (1996) 543

[31] C. Peterson, D. Schlatter, I. Schmitt and P.M. Zerwas: Phys. Rev. D27 (1983) 105

[32] J. Allison et al.: Nucl. Instrum. Methods A317 (1992) 47

[33] OPAL Coll., P.D. Acton et al.: Z. Phys. C56 (1992) 521

[34] OPAL Coll., R. Akers et al.: Z. Phys. C68 (1995) 1

[35] C. Beeston and R. Barlow: Comp. Phys. Commun. 77 (1993) 219

[36] See, for example, H.M. Wadsworth Jr. (Ed): *Handbook of Statistical Methods for Engineers and Physicists* (1989) (McGraw Hill)

[37] V. Blobel: in C. Verkerk (ed.), Proc. CERN School of Computing (Aiguablawa, Spain, September 1985), CERN 85-09

[38] OPAL Coll., G. Alexander et al.: Z. Phys. C72 (1996) 1

[39] OPAL Coll., K. Ackerstaff et al.: *A Measurement of the Charm and Bottom Forward-Backward Asymmetries using D mesons at LEP*, CERN PPE/96-101, submitted to Z. Phys. C

[40] OPAL Coll., R. Akers et al.: Z. Phys. C67 (1995) 27

[41] OPAL Coll., G. Alexander et al.: Phys. Lett. B364 (1995) 93

[42] OPAL Coll., R. Akers et al.: Z. Phys. C60 (1993) 199

[43] OPAL Coll., G. Alexander et al.: Phys. Lett. B262 (1991) 341

[44] ALEPH Coll., D. Decamp et al.: Phys. Lett. B244 (1990) 551;
ALEPH Coll., D. Decamp et al.: Phys. Lett. B266 (1991) 218;
DELPHI Coll., P. Abreu et al.: Z. Phys. C56 (1992) 47

[45] OPAL Coll., K. Ackerstaff et al.: *B^* production in Z^0 decays*, CERN-PPE/96-192, submitted to Phys. Lett. B

[46] OPAL Coll., G. Alexander et al.: Z. Phys. C66 (1995) 19

[47] ALEPH Coll., D. Buskulic et al.: *Production of orbitally excited charm mesons in semileptonic B decays*, CERN PPE/96-092, submitted to Z. Phys. C

[48] See for example I.G. Knowles et al.: in G. Altarelli, T. Sjöstrand and F. Zwirner (ed.), Physics at LEP 2, Vol. 2, CERN 96-01, p 103

[49] OPAL Coll., R. Akers et al.: Z. Phys. C66 (1995) 19

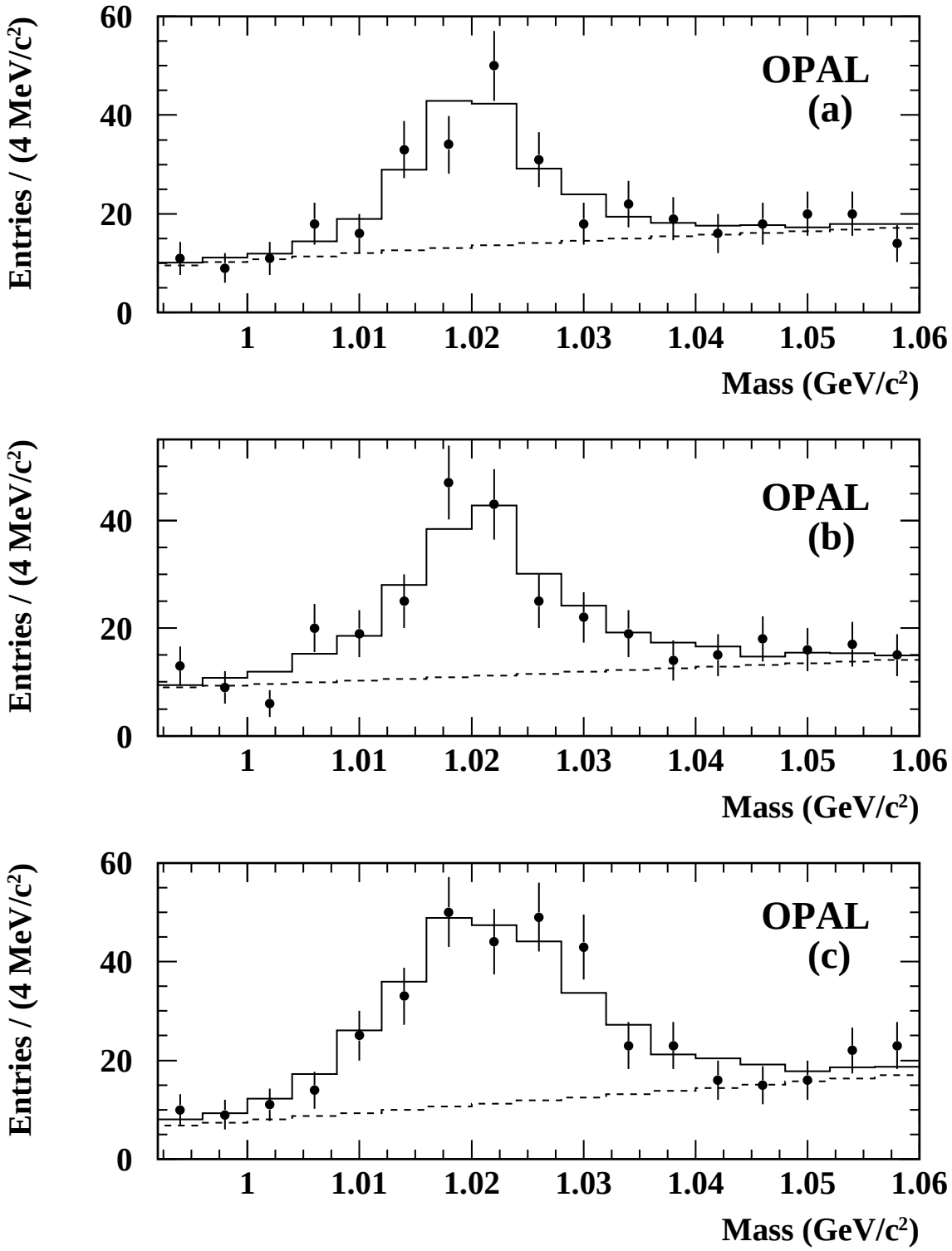

Figure 1: Two-particle invariant mass distribution of K^+K^- pairs with $x_E > 0.7$ in the ranges of decay angle (a) $0 \leq |\cos\theta_H| < 1/3$, (b) $1/3 \leq |\cos\theta_H| < 2/3$ and (c) $2/3 \leq |\cos\theta_H| \leq 1$. The points with error bars are the data. The solid histograms show the fits, with the background components shown separately as dashed histograms.

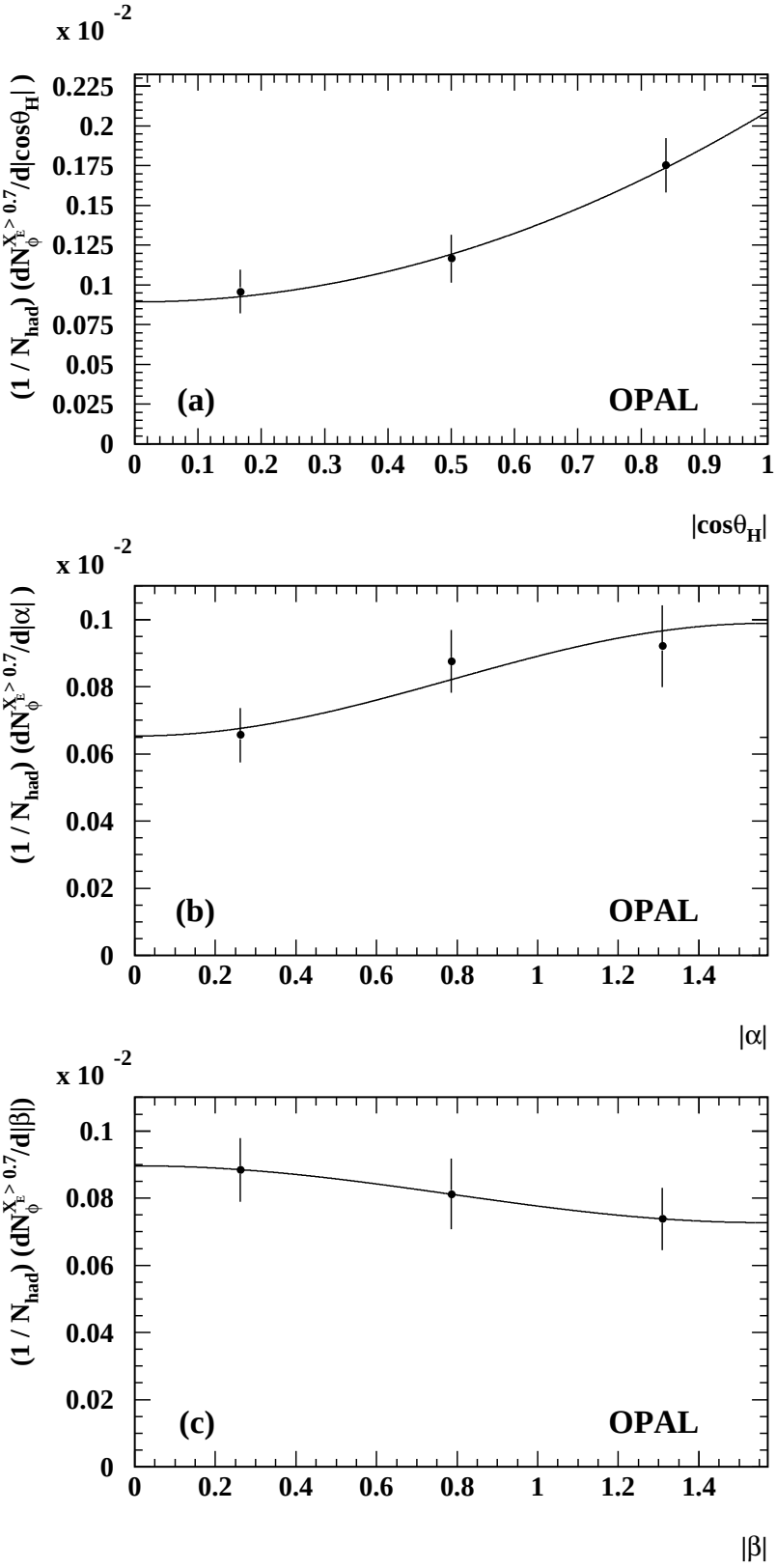

Figure 2: Corrected differential rates for ϕ mesons fitted to (a) $N(1-\rho_{00}+(3\rho_{00}-1)\cos^2\theta_{\rm H})$, (b) $N(1+2\ {\rm Re}\,\rho_{1-1}\cos 2|\alpha|)$, (c) $N(1+2\ {\rm Im}\,\rho_{1-1}\cos 2|\beta|)$, where the overall normalisation factors N and the spin density matrix elements are free parameters in the fits.

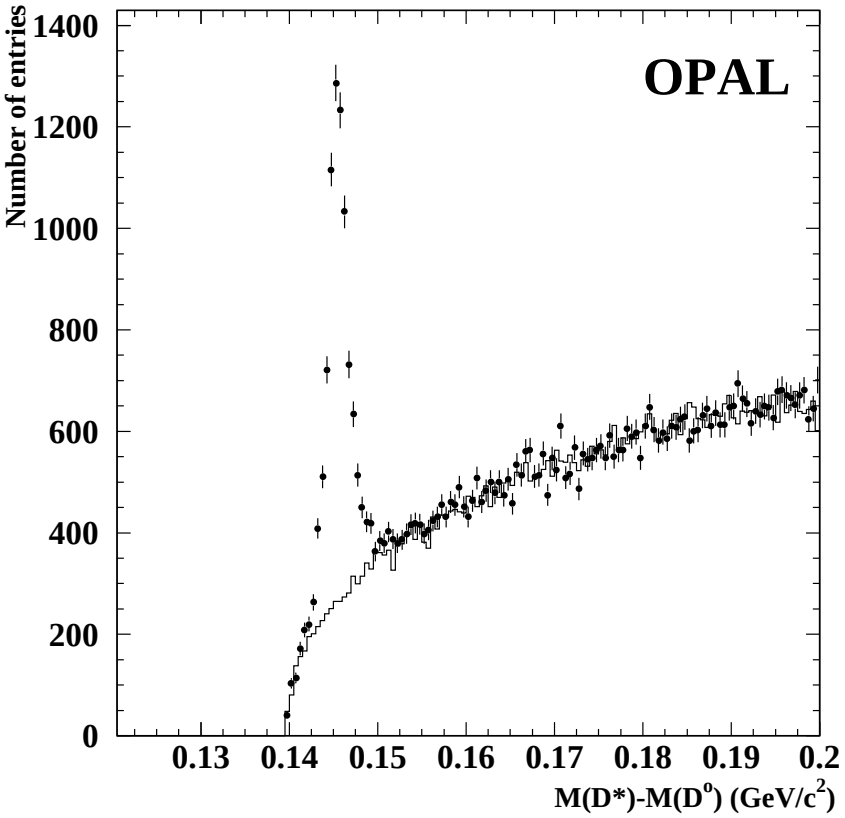

Figure 3: Mass difference distribution for the D^* candidates with $x_E > 0.2$, before applying the ΔM cut. The points show the signal sample and the line histogram the distribution of the background obtained from wrong-charge, reflected pion and reflected pion wrong-charge combinations. The errors on the data points are statistical only.

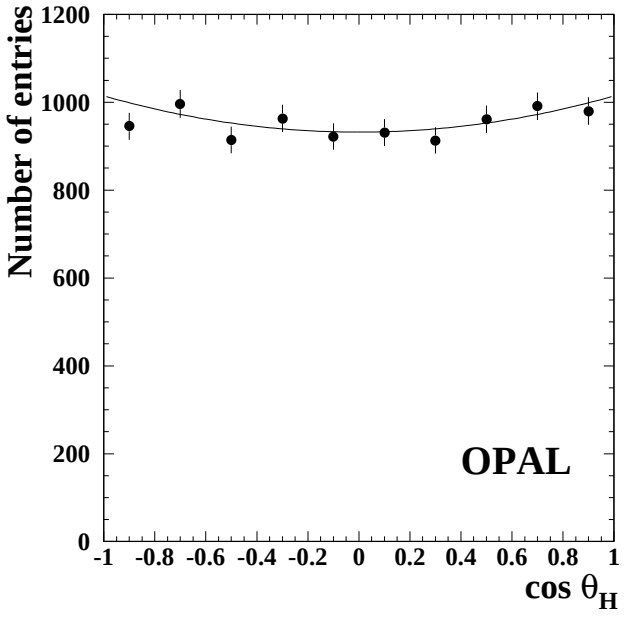

Figure 4: The $\cos\theta_{\rm H}$ distribution of all $\rm D^*$ candidates. The result of the 3 parameter log-likelihood fit for the spin alignment has been superimposed.

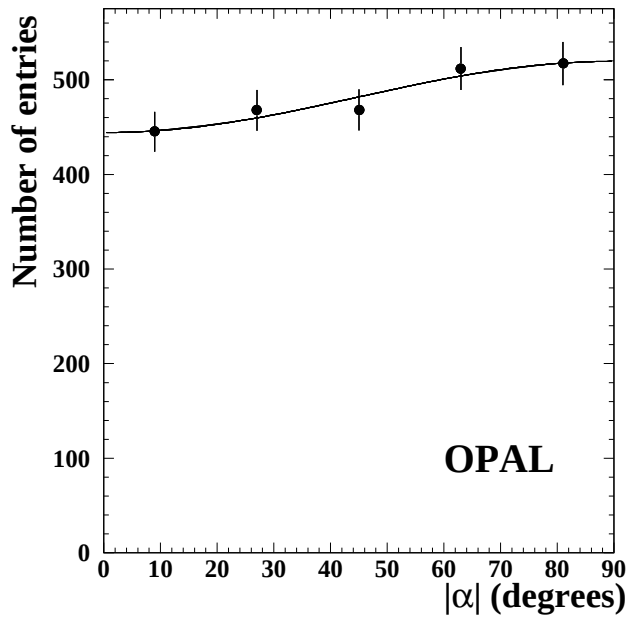

Figure 5: The $|\alpha|$ distribution of background subtracted $\rm D^*$ candidates for $x_E > 0.5$, fitted to $N(1 + 2{\rm Re}\,\rho_{1-1}\cos 2|\alpha|)$, where the overall normalisation factor N and the matrix element ${\rm Re}\,\rho_{1-1}$ are free parameters.

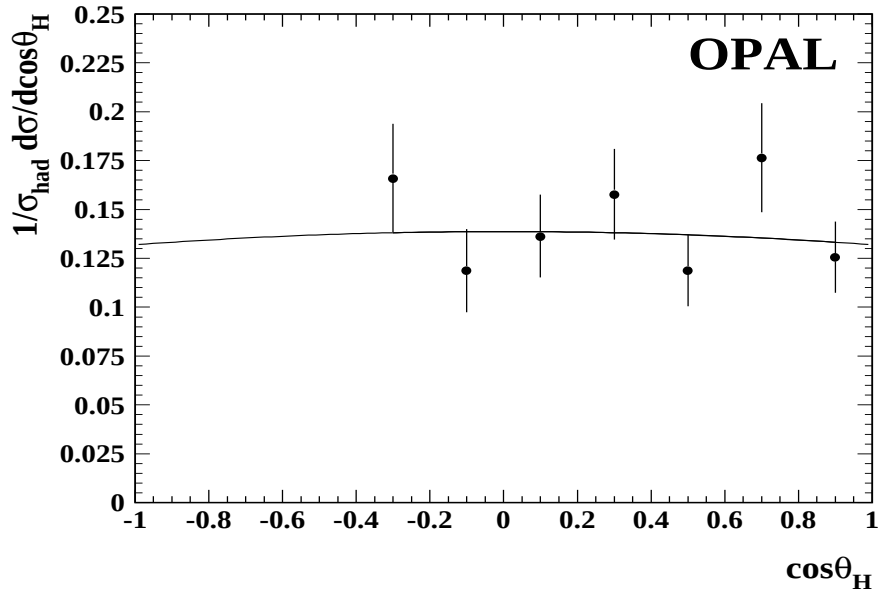

Figure 6: Polar angle distribution of the photon from B^* decay in the helicity frame, with the fit to the angular distribution of equation 8.